5+ model EABE : 1993 Prod.Type:FTP pp.1–20(col.fig.:1,4–21) ED:Dibyendu PAGN:Bala SCAN:

ARTICLE IN PRESS

ELSEVIER

Engineering Analysis with Boundary Elements ▮ (▮▮▮▮) ▮▮▮–▮▮▮

ENGINEERING ANALYSIS with BOUNDARY ELEMENTS

www.elsevier.com/locate/enganabound

Analytical study and numerical experiments of true and spurious eigensolutions of free vibration of circular plates using real-part BIEM

W.M. Lee[a], J.T. Chen[b,*]

[a]Department of Mechanical Engineering, China Institute of Technology, Taipei, Taiwan
[b]Department of Harbor and River Engineering, National Taiwan Ocean University, P.O. Box 7-59, Keelung 20224, Taiwan

Received 13 February 2007; received in revised form 17 September 2007; accepted 19 September 2007

Abstract

Following the success of the CHEEF method [Chen IL, Chen JT, Kuo SR, Liang MT. A new method for true and spurious eigensolutions of arbitrary cavities using the combined Helmholtz exterior integral equation formulation method. J Acoust Soc Am 2001; 109(3):982–98] and the real-part BEM [Kuo SR, Chen JT, Huang CX. Analytical study and numerical experiments for true and spurious eigensolutions of a circular cavity using the real-part dual BEM. Int J Numer Methods Eng 2000; 48:1401–22] for solving the membrane eigenproblem, we extend to the plate problem in this paper. The boundary integral equation method (BIEM) using only the real-part kernel instead of the complex-valued kernel is employed to solve the plate eigenproblem for saving half effort in computation. The spurious eigenvalue that resulted due to insufficient constraint is examined. To deal with this problem, a combined Helmholtz exterior integral equation formulation method (CHEEF) is employed to provide sufficient constraints to filter out spurious eigenvalues. The constraint equations of the transverse displacement, normal derivative and tangent derivative for the exterior collocating points are derived. If these constraint equations are properly chosen, one collocating point was sufficient to filter out all the spurious eigenvalues easily and efficiently, even for the repeated spurious eigenvalues. Finally, numerical experiments are performed to verify the analytical results.

Keywords: Boundary integral equation method; Circular plate; Spurious eigenvalue; Degenerate kernel; Fourier series; SVD; CHEEF method

1. Introduction

For the simply-connected eigenproblem, it is well known that either the real-part or imaginary-part boundary integral equations (BIEs) result in spurious eigenvalues [1]. De Mey [2,3], Yas'ko [4], Hutchinson and Wong [5–7] employed only the real-part kernel to solve the membrane and plate vibrations free of the complex-valued computation in sacrifice of occurrence of spurious solutions. Hutchinson [8] presented a direct BEM for plate vibration involving displacement, slope, moment and shear force. They were able to obtain numerical results for clamped plates by employing only the real-part BEM with obvious computational gains. However, this saving leads to spurious eigenvalues in addition to true ones for free vibration analysis. One has to investigate the mode shapes in order to identify and reject the spurious ones. Shaw [9] commented that using only the real-part kernel was incorrect since the characteristic equation must satisfy the real-part and imaginary-part equations at the same time. Hutchinson [10] replied that the claim of incorrectness was perhaps a little strong, since the real-part BEM does not miss any true eigenvalue, although the solution is contaminated by spurious ones according to numerical experiences. However, no proof was provided at that time. Until 2000, Chen and his coworkers [11] proved the existence of spurious eigenvalues and pointed out that they are zeros of Bessel function of the second kind through a circular membrane for the real-part DBEM. Niwa et al. [12] also stated that "One must take care to use the

*Corresponding author.
E-mail address: jtchen@mail.ntou.edu.tw (J.T. Chen).

0955-7997/$ - see front matter © 2007 Elsevier Ltd. All rights reserved.
doi:10.1016/j.enganabound.2007.09.004

complete Green's function for outgoing waves, as attempts to use only the real (singular) or imaginary (regular) part separately will not provide the complete spectrum". As quoted from the reply of Hutchinson [10], this comment is not correct since the real-part BEM does not lose any true eigenvalue. The reason is that the real-part and imaginary-part kernels satisfy the Hilbert transform pair. They are not fully independent. To use both parts, real and imaginary kernels may be not economical in computation. Complete eigenspectrum is imbedded in either real or imaginary-part kernel. If we usually need to look for the eigenmode as well as eigenvalue, the sorting for the spurious solutions pay a small overhead by identifying the mode shapes. Chen et al. [13] commented that the nodal line of spurious modes may be reasonable which could mislead the judgments of the true and spurious ones, since the true and spurious modes may have the same nodal line in case of different eigenvalues. This is why Chen and his coworkers have developed several techniques, e.g., dual formulation [13], domain partition [14], singular value decomposition (SVD) updating technique [15], combined Helmholtz exterior equation formulation (CHEEF) method [16] for sorting out true and spurious eigenvalues. The main concept of these techniques to treat spurious or fictitious frequency is to provide sufficient constrains to overcome the rank deficiency of the system due to boundary integral formulation. For a simply-connected eigenproblem, the complex-valued boundary integral formulation can offer sufficient constraints and spurious eigenvalue does not appear. Even though the complex-valued BEM is employed, spurious eigenvalue may also appear for multiply-connected problems [17,18]. For plate dynamics using BEM, readers may consult with one book and two review articles [19–21].

Using the dual MRM or the real-part dual BEM, spurious eigenvalues can be filtered out by checking the residue between the singular and hypersingular equations [22]. Both the dual MRM [23] method and the real-part dual BEM [15] in conjunction with the SVD technique must calculate a matrix with dimension $4N$ by $2N$, where $2N$ is the number of elements. For the exterior acoustics, complex-valued integral equation formulations usually result in fictitious frequencies. Schenck [24] proposed a combined Helmholtz interior integral equation formulation (CHIEF) method to suppress fictitious frequencies using additional constraints provided by null-field integral equation by collocating interior points. Recently, some results [25] on the annular plate with the CHIEF method have been reported. Based on the concept of the CHIEF method, the CHEEF method has been successively applied to the membrane eigenproblem [16]. By applying the CHEEF method to the plate problem, the missing constraints can be recovered by applying the integral equations on a number of points located outside the domain. Namely, constraints can be provided from null-field integral equations [26]. Only a matrix with matrix dimension $(2N+1)$ by $2N$ or $(2N+2)$ by $2N$ for CHEEF instead of $4N$ by $2N$ in dual formulation is required. The gain of smaller size of matrix is obvious.

In this study, we will employ the CHEEF method to filter out spurious solutions for circular plate eigenproblems. The selection of constraint equations for the number and position of the exterior points will be examined analytically and verified numerically. After assembling the CHEEF equations, an SVD technique [27] is employed to determine the eigenvalues, multiplicity and boundary modes. The boundary modes can be extracted easily from the right unitary matrix using SVD with respect to the influence matrix. The equations of constraint in the transverse displacement, normal derivative and tangent derivative for the exterior collocating points were employed to increase the rank such that spurious eigenvalues can be easily and efficiently filtered out.

2. Boundary integral equations for a plate eigenproblem

The governing equation for the free flexural vibration of a uniform thin plate is shown as follows:

$$\nabla^4 u(x) = \lambda^4 u(x), \quad x \in \Omega \tag{1}$$

where u is the lateral displacement, λ is the frequency parameter ($\lambda^4 = \omega^2 \rho_0 h/D$), ω is the circular frequency, ρ_0 is the volume density, D is the flexural rigidity expressed as $D = Eh^3/12(1-v^2)$ in terms of the Young's modulus E, the Poisson ratio v and the plate thickness h, and Ω is the domain of the thin plate.

The integral representation for the plate eigenproblem can be derived from the Rayleigh–Green identity [19] as follows:

$$\begin{aligned} u(x) = & -\int_B U(s,x)v(s)\,\mathrm{d}B(s) + \int_B \Theta(s,x)m(s)\,\mathrm{d}B(s) \\ & -\int_B M(s,x)\,\theta(s)\,\mathrm{d}B(s) + \int_B V(s,x)u(s)\,\mathrm{d}B(s), \quad x \in \Omega \end{aligned} \tag{2}$$

$$\begin{aligned} \theta(x) = & -\int_B U_\theta(s,x)v(s)\,\mathrm{d}B(s) + \int_B \Theta_\theta(s,x)m(s)\,\mathrm{d}B(s) \\ & -\int_B M_\theta(s,x)\theta(s)\,\mathrm{d}B(s) + \int_B V_\theta(s,x)u(s)\,\mathrm{d}B(s), \quad x \in \Omega \end{aligned} \tag{3}$$

Please cite this article as: Lee WM, Chen JT. Analytical study and numerical experiments of true and spurious eigensolutions of free vibration of circular plates using real-part.... Eng Anal Bound Elem (2007), doi:10.1016/j.enganabound.2007.09.004

$$m(x) = -\int_B U_m(s,x)v(s)\,\mathrm{d}B(s) + \int_B \Theta_m(s,x)m(s)\,\mathrm{d}B(s) - \int_B M_m(s,x)\theta(s)\,\mathrm{d}B(s) + \int_B V_m(s,x)u(s)\,\mathrm{d}B(s), \quad x \in \Omega \tag{4}$$

$$v(x) = -\int_B U_v(s,x)v(s)\,\mathrm{d}B(s) + \int_B \Theta_v(s,x)m(s)\,\mathrm{d}B(s) - \int_B M_v(s,x)\theta(s)\,\mathrm{d}B(s) + \int_B V_v(s,x)u(s)\,\mathrm{d}B(s), \quad x \in \Omega \tag{5}$$

where B is the boundary of the domain Ω, $u(x), \theta(x), m(x)$ and $v(x)$ are the displacement, slope, moment and shear force, s and x mean the source and field points, respectively. The kernel functions U, Θ, M, V, U_θ, Θ_θ, M_θ, V_θ, U_m, Θ_m, M_m, V_m, U_v, Θ_v, M_v and V_v in Eqs. (2)–(5) can be expanded to degenerate kernels by separating the source and field points and will be elaborated on later. The kernel function $U_c(s,x)$ in Eq. (2) is the fundamental solution which satisfies

$$\nabla^4 U_c(s,x) - \lambda^4 U_c(s,x) = \delta(s-x), \tag{6}$$

where ∇^4 is the biharmonic operator and $\delta(s-x)$ is the Dirac–δ function, respectively. Considering the two singular solutions ($Y_0(\lambda r)$ and $K_0(\lambda r)$, which are the zeroth-order of the second-kind Bessel and modified Bessel functions, respectively) [8] and two regular solutions ($J_0(\lambda r)$ and $I_0(\lambda r)$, which are the zeroth-order of the first-kind Bessel and modified Bessel functions, respectively) in the fundamental solution, we have the complex-valued kernel,

$$c(s,x) = \frac{1}{8\lambda^2}\left[Y_0(\lambda r) + iJ_0(\lambda r) + \frac{2}{\pi}(K_0(\lambda r) + iI_0(\lambda r))\right], \tag{7}$$

where $r \equiv |s-x|$ and $i^2 = -1$. By selecting the real-part kernel of $U_c(s,x)$ as the kernel $U(s,x)$, the other three kernels, $\Theta(s,x)$, $M(s,x)$ and $V(s,x)$ in Eq. (2) can be obtained by applying the following slope, moment and effective shear operators defined by

$$K_\Theta = \frac{\partial(\cdot)}{\partial n} \tag{8}$$

$$K_M = \nu\nabla^2(\cdot) + (1-\nu)\frac{\partial^2(\cdot)}{\partial n^2} \tag{9}$$

$$K_V = \frac{\partial}{\partial n}\nabla^2(\cdot) + (1-\nu)\frac{\partial}{\partial t}\left[\frac{\partial}{\partial n}\left(\frac{\partial}{\partial t}(\cdot)\right)\right] \tag{10}$$

to the kernel $U(s,x)$ with respect to the source point, where $\partial/\partial n$ and $\partial/\partial t$ are the normal and tangential derivatives, respectively, and ∇^2 means the Laplacian operator. In the polar coordinate of (R,θ), the normal and tangential derivatives can be expressed by $\partial/\partial R$ and $(\partial/\partial R)(\partial/\partial\theta)$, respectively, and then the three kernel functions can be rewritten as

$$\Theta(s,x) = K_{\Theta,s}(U(s,x)) = \frac{\partial U(s,x)}{\partial R} \tag{11}$$

$$M(s,x) = K_{M,s}(U(s,x)) = \nu\nabla_s^2 U(s,x) + (1-\nu)\frac{\partial^2 U(s,x)}{\partial R^2}s \tag{12}$$

$$V(s,x) = K_{V,s}(U(s,x)) = \frac{\partial}{\partial R}\left(\nabla_s^2 U(s,x)\right) + (1-\nu)\left(\frac{1}{R}\right)\frac{\partial}{\partial\theta}\left[\frac{\partial}{\partial R}\left(\frac{1}{R}\frac{\partial U(s,x)}{\partial\theta}\right)\right]. \tag{13}$$

The expressions for $\theta(x), m(x)$ and $v(x)$ in Eqs. (3)–(5), which can be obtained by applying the operators in Eqs. (8)–(10) to $u(x)$ in Eq. (2) with respect to the field point $x(\rho,\phi)$, are

$$\theta(x) = K_{\Theta,x}(u(x)) = \frac{\partial u(x)}{\partial\rho}, \tag{14}$$

$$m(x) = K_{M,x}(u(x)) = \nu\nabla^2 u(x) + (1-\nu)\frac{\partial^2 u(x)}{\partial\rho^2}, \tag{15}$$

$$v(x) = K_{V,x}(u(x)) = \frac{\partial}{\partial\rho}(\nabla_s^2 u(x)) + (1-\nu)\left(\frac{1}{\rho}\right)\frac{\partial}{\partial\phi}\left[\frac{\partial}{\partial\rho}\left(\frac{1}{\rho}\frac{\partial u(x)}{\partial\phi}\right)\right], \tag{16}$$

Please cite this article as: Lee WM, Chen JT. Analytical study and numerical experiments of true and spurious eigensolutions of free vibration of circular plates using real-part.... Eng Anal Bound Elem (2007), doi:10.1016/j.enganabound.2007.09.004

In this way, the kernel functions U_θ, Θ_θ, M_θ, V_θ, U_m, Θ_m, M_m, V_m, U_v, Θ_v, M_v and V_v can be obtained by applying the operators in Eqs. (8)–(10) to U, Θ, M and V with respect to the field point $x(\rho,\phi)$.

The null-field integral equations for the null field point (including the boundary point if exterior degenerate kernels are adopted) are shown as follows:

$$0 = -\int_B U(s,x)v(s)\,\mathrm{d}B(s) + \int_B \Theta(s,x)m(s)\,\mathrm{d}B(s) - \int_B M(s,x)\theta(s)\,\mathrm{d}B(s) + \int_B V(s,x)u(s)\,\mathrm{d}B(s), \quad x \in \Omega^C \cup B, \tag{17}$$

$$0 = -\int_B U_\theta(s,x)v(s)\,\mathrm{d}B(s) + \int_B \Theta_\theta(s,x)m(s)\,\mathrm{d}B(s) - \int_B M_\theta(s,x)\theta(s)\,\mathrm{d}B(s) + \int_B V_\theta(s,x)u(s)\,\mathrm{d}B(s), \quad x \in \Omega^C \cup B, \tag{18}$$

$$0 = -\int_B U_m(s,x)v(s)\,\mathrm{d}B(s) + \int_B \Theta_m(s,x)m(s)\,\mathrm{d}B(s) - \int_B M_m(s,x)\theta(s)\,\mathrm{d}B(s) + \int_B V_m(s,x)u(s)\,\mathrm{d}B(s), \quad x \in \Omega^C \cup B, \tag{19}$$

$$0 = -\int_B U_v(s,x)v(s)\,\mathrm{d}B(s) + \int_B \Theta_v(s,x)m(s)\,\mathrm{d}B(s) - \int_B M_v(s,x)\theta(s)\,\mathrm{d}B(s) + \int_B V_v(s,x)u(s)\,\mathrm{d}B(s), \quad x \in \Omega^C \cup B, \tag{20}$$

where Ω^C is the complementary domain of Ω. It is a closed set since B can be included. Since the four equations of Eqs. (17)–(20) in the plate formulation are provided, there are 6 (C_2^4) options for choosing any two equations to solve the problems. For simplicity, the Eqs. (17) and (18) are used here to analyze the plate problems. In the real implementation, the point in the null-field integral equation can be exactly located on the real boundary, B, while kernel functions are expressed in proper degenerate forms. Consequently, all the improper integrals disappear and transform to series sum in the BIEs since the potential across the boundary can be explicitly determined in both sides using degenerate kernels. Successful experiences on Laplace problems and biharmonic problems can be found in [1,26].

The displacement $u(s)$, slope $\theta(s)$, moment $m(s)$ and shear force $v(s)$ along the circular boundaries in the null-field integral equations are expanded in terms of Fourier series, respectively, as shown below:

$$u(s) = c_0 + \sum_{n=1}^{M}(c_n \cos n\theta + d_n \sin n\theta), \quad s \in B, \tag{21}$$

$$\theta(s) = g_0 + \sum_{n=1}^{M}(g_n \cos n\theta + h_n \sin n\theta), \quad s \in B, \tag{22}$$

$$m(s) = a_0 + \sum_{n=1}^{M}(a_n \cos n\theta + b_n \sin n\theta), \quad s \in B, \tag{23}$$

$$v(s) = p_0 + \sum_{n=1}^{M}(p_n \cos n\theta + q_n \sin n\theta), \quad s \in B, \tag{24}$$

where $a_0, a_n, b_n, c_0, c_n, d_n, g_0, g_n, h_n, p_0, p_n$ and q_n are the Fourier coefficients and M is the number of Fourier series terms.

In the polar coordinate, the field point and source point can be expressed as (ρ,ϕ) and (R,θ), respectively. By employing the separation technique for the source and field points, the kernel functions $U(s,x)$ and $\Theta(s,x)$ are expanded in the series form as follows:

Please cite this article as: Lee WM, Chen JT. Analytical study and numerical experiments of true and spurious eigensolutions of free vibration of circular plates using real-part.... Eng Anal Bound Elem (2007), doi:10.1016/j.enganabound.2007.09.004

$$U(s,x)=\frac{1}{8\lambda^2}\left[Y_0(\lambda r)+\frac{2}{\pi}K_0(\lambda r)\right]$$
$$=\begin{cases}U^I(s,x)=\frac{1}{8\lambda^2}\sum_{m=0}^{\infty}\varepsilon_m\{J_m(\lambda\rho)\,Y_m(\lambda R)+\frac{2}{\pi}I_m(\lambda\rho)K_m(\lambda R)\}\cos(m(\theta-\phi)), & R\geqslant\rho\\ U^E(s,x)=\frac{1}{8\lambda^2}\sum_{m=0}^{\infty}\varepsilon_m\{J_m(\lambda R)\,Y_m(\lambda\rho)+\frac{2}{\pi}I_m(\lambda R)K_m(\lambda\rho)\}\cos(m(\theta-\phi)), & \rho>R\end{cases} \tag{25a, b}$$

$$\Theta(s,x)=\frac{\partial U(s,x)}{\partial R}$$
$$=\begin{cases}\Theta^I(s,x)=\frac{1}{8\lambda}\sum_{m=0}^{\infty}\varepsilon_m\{J_m(\lambda\rho)\,Y'_m(\lambda R)+\frac{2}{\pi}I_m(\lambda\rho)K'_m(\lambda R)\}\cos(m(\theta-\phi)), & R\geqslant\rho\\ \Theta^E(s,x)=\frac{1}{8\lambda}\sum_{m=0}^{\infty}\varepsilon_m\{J'_m(\lambda R)\,Y_m(\lambda\rho)+\frac{2}{\pi}I'_m(\lambda R)K_m(\lambda\rho)\}\cos(m(\theta-\phi)), & \rho>R\end{cases} \tag{26a, b}$$

where the superscripts "I" and "E" denote the interior and exterior cases of $U(s,x)$ kernel. The other kernels in the boundary integral equations can be obtained by utilizing the operators of Eqs. (8)–(10) with respect to the $U(s,x)$ kernel. The degenerate kernels M and V in Eqs. (17) are listed in Appendix A. The kernel function with the superscript "I" is chosen while the field point is inside the circular region; otherwise, the kernels with the superscript "E" are chosen.

For the clamped circular plate ($u=0$ and $\theta=0$) with a radius a, the moment and shear force, $m(s)$ and $v(s)$, are expanded into Fourier series as shown in Eqs. (23) and (24).

By substituting the degenerate kernels, Eqs. (25) and (26), into Eqs. (17) on the boundary ($\rho=R=a$), we have

$$\begin{aligned}0=&-\int_B U(s,x)v(s)\,\mathrm{d}B(s)+\int_B\Theta(s,x)m(s)\,\mathrm{d}B(s)\\ =&-\int_B\left(\frac{1}{8\lambda^2}\sum_{m=0}^{\infty}\varepsilon_m\left\{J_m(\lambda a)\,Y_m(\lambda a)+\frac{2}{\pi}I_m(\lambda a)K_m(\lambda a)\right\}\cos(m(\theta-\phi))\right)\\ &\times\left(a_0+\sum_{n=1}^{M}(a_n\cos n\theta+b_n\sin n\theta)\right)\mathrm{d}B(s)+\int_B\left(\frac{1}{8\lambda}\sum_{m=0}^{\infty}\varepsilon_m\left\{J_m(\lambda a)\,Y'_m(\lambda a)\right.\right.\\ &\left.\left.+\frac{2}{\pi}I_m(\lambda a)K'_m(\lambda a)\right\}\cos(m(\theta-\phi))\left(p_0+\sum_{n=1}^{M}(p_n\cos n\theta+q_n\sin n\theta)\right)\mathrm{d}B(s)\right.\end{aligned} \tag{27}$$

According to the orthogonal property, Eq. (27) can be rewritten as

$$\begin{aligned}0=&-\frac{\pi a}{4\lambda^2}\left(\sum_{m=0}^{M}\left\{J_m(\lambda a)\,Y_m(\lambda a)+\frac{2}{\pi}I_m(\lambda a)K_m(\lambda a)\right\}\right.\\ &\times(a_m\cos m\phi+b_m\sin m\phi))+\frac{\pi a}{4\lambda^2}\left(\sum_{m=0}^{M}\left\{J_m(\lambda a)\,Y'_m(\lambda a)\right.\right.\\ &\left.\left.+\frac{2}{\pi}I_m(\lambda a)K'_m(\lambda a)\right\}(p_m\cos m\phi+q_m\sin m\phi)\right).\end{aligned} \tag{28}$$

Since Eq. (28) is valid for any ϕ, we have

$$\left\{J_m(\lambda a)\,Y_m(\lambda a)+\frac{2}{\pi}I_m(\lambda a)K_m(\lambda a)\right\}a_m+\left\{J_m(\lambda a)\,Y'(\lambda a)+\frac{2}{\pi}I_m(\lambda a)K'_m(\lambda a)\right\}p_m=0, \tag{29}$$

$$\left\{J_m(\lambda a)\,Y_m(\lambda a)+\frac{2}{\pi}I_m(\lambda a)K_m(\lambda a)\right\}b_m+\left\{J_m(\lambda a)\,Y'(\lambda a)+\frac{2}{\pi}I_m(\lambda a)K'_m(\lambda a)\right\}q_m=0. \tag{30}$$

Similarly, Eq. (18) yields

$$\left\{J'_m(\lambda a)\,Y_m(\lambda a)+\frac{2}{\pi}I'_m(\lambda a)K_m(\lambda a)\right\}a_m+\left\{J'_m(\lambda a)\,Y'(\lambda a)+\frac{2}{\pi}I'_m(\lambda a)K'_m(\lambda a)\right\}p_m=0, \tag{31}$$

$$\left\{J'_m(\lambda a)\,Y_m(\lambda a)+\frac{2}{\pi}I'_m(\lambda a)K_m(\lambda a)\right\}b_m+\left\{J'_m(\lambda a)\,Y'(\lambda a)+\frac{2}{\pi}I'_m(\lambda a)K'_m(\lambda a)\right\}q_m=0. \tag{32}$$

Please cite this article as: Lee WM, Chen JT. Analytical study and numerical experiments of true and spurious eigensolutions of free vibration of circular plates using real-part.... Eng Anal Bound Elem (2007), doi:10.1016/j.enganabound.2007.09.004

To seek nontrivial data for the generalized coefficients of a_m, b_m, p_m and q_m, we can obtain the eigenequations by using either Eqs. (29) and (31) or Eqs. (30) and (32)

$$\frac{J_m(\lambda a)Y_m(\lambda a)+(2/\pi)I_m(\lambda a)K_m(\lambda a)}{J'_m(\lambda a)Y_m(\lambda a)+(2/\pi)I'_m(\lambda a)K_m(\lambda a)}=\frac{J_m(\lambda a)Y'(\lambda a)+(2/\pi)I_m(\lambda a)K'_m(\lambda a)}{J'_m(\lambda a)Y'(\lambda a)+(2/\pi)I'_m(\lambda a)K'_m(\lambda a)}. \tag{33}$$

After recollecting the terms, Eq. (33) can be simplified to

$$m(\lambda a)Y_{m+1}(\lambda a)-K_{m+1}(\lambda a)Y_m(\lambda a)]\times\{I_{m+1}(\lambda a)J_m(\lambda a)+I_m(\lambda a)J_{m+1}(\lambda a)\}=0. \tag{34}$$

The former part in Eq. (34) inside the bracket is the spurious eigenequation, while the latter part inside the brace is found to be the true eigenequation after comparing with the exact eigenequation [28].

By selecting finite terms of the Fourier series representation in Eqs. (21)–(24) and uniformly collocating sufficient points on the boundary, a linear algebraic system can be constructed by using Eqs. (17)–(20) in conjunction with the degenerate kernel. The direct searching approach [19] is employed to determine the natural frequency of parameters through singular value decomposition (SVD). The right unitary vector in SVD is the boundary mode, i.e., the Fourier coefficients in Eqs. (21)–(24). The mode shape can be obtained by substituting the boundary mode into the integral representation for the field point of Eq. (2). For the clamped case, a linear algebraic system can be expressed as

$$\begin{bmatrix} U\Theta \\ U_\theta\Theta_\theta \end{bmatrix}_{4N\times 4N}\begin{Bmatrix} v \\ m \end{Bmatrix}_{4N\times 1}=\begin{Bmatrix} 0 \\ 0 \end{Bmatrix}_{4N\times 1}. \tag{35}$$

3. CHEEF treatment for spurious eigensolution

Following the success of CHEEF method to suppress spurious eigenvalue for membrane eigenproblems [16], the CHEEF method is adopted to suppress the occurrence of the spurious eigenvalues for the free vibration of plate problem. A clamped case is demonstrated for simplicity. By substituting the real-part degenerate kernels of Eqs. (25a) and (26a) for the interior point ($0<\rho<\psi a$), the Fourier expansions for the moment and effect shear and the relationship between the Fourier coefficients (i.e. Eq. (29) and Eq. (30)), into the integral representation for the displacement $u(x)$ of Eq. (2), we have

$$\begin{aligned} u_m(\rho,\phi)=\frac{1}{2\pi\lambda^2}\Bigg(&\frac{1}{J'_m(\lambda a)Y_m(\lambda a)+(2/\pi)I'_m(\lambda a)K_m(\lambda a)}(I_m(\lambda\rho)(2K_m(\lambda a)+\lambda a\pi(J_m(\lambda a)K_{m+1}(\lambda a)\\ &-J_{m+1}(\lambda a)K_m(\lambda a))Y_m(\lambda a))+\pi J_m(\lambda\rho)((\lambda aI_{m+1}(\lambda a)K_m(\lambda a)-1)Y_m(\lambda a)\\ &+\lambda aI_m(\lambda a)K_m(\lambda a)Y_{m+1}(\lambda a))\Bigg)(a_m\cos m\phi+b_m\sin m\phi),\quad 0<\rho<a,\quad 0\leqslant\phi<2\pi \end{aligned} \tag{36}$$

Similarly, for the null-field equation ($\rho>a$) of Eq. (17) yields

$$\begin{aligned} 0=\frac{a}{2\lambda}\Bigg(&\frac{(I_{m+1}(\lambda a)J_m(\lambda a)+I_m(\lambda a)J_{m+1}(\lambda a))[K_m(\lambda\rho)Y_m(\lambda a)-K_m(\lambda a)Y_m(\lambda\rho)]}{\{J'_m(\lambda a)Y_m(\lambda a)+(2/\pi)I'_m(\lambda a)K_m(\lambda a)\}}\Bigg)\\ &\times(a_m\cos m\phi+b_m\sin m\phi)\quad \rho>a,\quad 0\leqslant\phi<2\pi, \end{aligned} \tag{37}$$

Since the true eigenvalue λ_t satisfies $I_{m+1}(\lambda_t a)J_m(\lambda_t a)+I_m(\lambda_t a)J_{m+1}(\lambda_t a)=0$, we can find that the field of the interior ($\rho<a$) and exterior ($\rho>a$) points are the nontrivial mode (Eq. (36)) and null-field (Eq. (37)), respectively. It is found that the solution of the exterior point ($\rho>a$) is not a null-field in Eq. (37) for the spurious eigenvalue λ_s which satisfies $K_m(\lambda_s a)Y_{m+1}(\lambda_s a)-K_{m+1}(\lambda_s a)Y_m(\lambda_s a)=0$. This provides us a clue to filter out spurious eigenvalue. In this way, the null-field equations can be selected as independent constraints to suppress the occurrence of the spurious eigenvalues for the plate eigenproblem. In other words, Eq. (37) can be employed to increase the rank once the null-field equation is not satisfied. Similarly, the nontrivial normal derivative $\theta(x)$ and tangent derivative $t(x)$ of the exterior points can also be employed to provide additional independent constraints as shown below:

$$\begin{aligned} 0=&-\frac{a\lambda}{4}\Bigg(\frac{(I_{m+1}(\lambda a)J_m(\lambda a)+I_m(\lambda a)J_{m+1}(\lambda a))}{\{J'_m(\lambda a)Y_m(\lambda a)+(2/\pi)I'_m(\lambda a)K_m(\lambda a)\}}\Bigg)\\ &\times[K_m(\lambda a)Y_{m-1}(\lambda\rho)+K_{m-1}(\lambda\rho)Y_m(\lambda a)+K_{m+1}(\lambda\rho)Y_m(\lambda a)-K_m(\lambda a)Y_{m+1}(\lambda\rho)]\\ &\times(a_m\cos m\phi+b_m\sin m\phi),\quad \rho>a,\quad 0\leqslant\phi<2\pi, \end{aligned} \tag{38}$$

Please cite this article as: Lee WM, Chen JT. Analytical study and numerical experiments of true and spurious eigensolutions of free vibration of circular plates using real-part.... Eng Anal Bound Elem (2007), doi:10.1016/j.enganabound.2007.09.004

$$0 = \frac{a}{2\lambda}\left(\frac{m}{\rho}\right)\left(\frac{(I_{m+1}(\lambda a)J_m(\lambda a) + I_m(\lambda a)J_{m+1}(\lambda a))(K_m(\lambda\rho)Y_m(\lambda a) - K_m(\lambda a)Y_m(\lambda\rho))}{\{J'_m(\lambda a)Y_m(\lambda a) + (2/\pi)I'_m(\lambda a)K_m(\lambda a)\}}\right)$$
$$\times (b_m \cos m\phi - a_m \sin m\phi), \quad \rho > a, \quad 0 \leqslant \phi < 2\pi. \tag{39}$$

In this section, we employ the CHEEF method to deal with the problem of spurious eigenvalues. Firstly, we choose a CHEEF point (ρ_1, ϕ_1) outside the domain $(\rho_1 > a, 0 \leqslant \phi_1 < 2\pi)$ and substitute the CHEEF point (ρ_1, ϕ_1) into Eq. (37) to get

$$0 = \frac{a}{2\lambda}\left(\frac{(I_{m+1}(\lambda a)J_m(\lambda a) + I_m(\lambda a)J_{m+1}(\lambda a))[K_m(\lambda\rho_1)Y_m(\lambda a) - K_m(\lambda a)Y_m(\lambda\rho_1)]}{\{J'_m(\lambda a)Y_m(\lambda a) + (2/\pi)I'_m(\lambda a)K_m(\lambda a)\}}\right)$$
$$(a_m \cos m\phi_1 + b_m \sin m\phi_1), \quad \rho_1 > a, \quad 0 \leqslant \phi_1 < 2\pi. \tag{40}$$

Comparing with the true eigenequation $I_{m+1}(\lambda a)J_m(\lambda a) + I_m(\lambda a)J_{m+1}(\lambda a) = 0$, Eq. (40) shows the null field as expected when $\rho_1 > a$. On the other hand, the spurious eigenvalue is not the case. In this way, Eq. (40) can provide the independent constraint to suppress the spurious eigensolution if $K_m(\lambda_s\rho_1)Y_m(\lambda_s a) - K_m(\lambda_s a)Y_m(\lambda_s\rho_1) \neq 0$ where λ_s satisfies$K_m(\lambda_s a)Y_{m+1}(\lambda_s a) - K_{m+1}(\lambda_s a)Y_m(\lambda_s a) = 0$. The CHEEF point (ρ_1, ϕ_1) may fail in adding independent equations, while $K_m(\lambda_s\rho_1)Y_m(\lambda_s a) - K_m(\lambda_s a)Y_m(\lambda_s\rho_1) = 0$. The reason is that we get a trivial constraint equation. The possible failure positions of $\rho_f$which satisfy $K_m(\lambda_s\rho_f)Y_m(\lambda_s a) - K_m(\lambda_s a)Y_m(\lambda_s\rho_f) = 0$ are shown in Table 1 for null-field equation of displacement. For the mode type (m, n) in Table 1, m denotes the number of diametrical nodes and n denotes the number of circular nodes for interior mode and for radiation mode, respectively. Similarly, by considering the normal derivative constrains, the possible failure positions of ρ_f which satisfies $K_m(\lambda_s a)Y_{m-1}(\lambda_s\rho_f) + K_{m-1}(\lambda_s\rho_f)Y_m(\lambda_s a) + K_{m+1}(\lambda_s\rho_f)Y_m(\lambda_s a) - K_m(\lambda_s a)Y_{m+1}(\lambda_s\rho_f) = 0$ are shown in Table 2. By comparing Eq. (37) with Eq. (39), the possible failure positions of the tangent derivative constraint are the same as those of the displacement constraint in Table 1.

Because one added point supplies at most one independent constraint, an additional point is required for the spurious eigenvalues of multiplicity two. In order to obtain sufficient constraints, we add another point (ρ_2, ϕ_2) in the exterior domain $(\rho_2 > a, 0 \leqslant \phi_2 < 2\pi)$. By substituting this field point (ρ_2, ϕ_2) into Eq. (37), we have

$$0 = \frac{a}{2\lambda}\sum_{m=0}^{M}\left(\frac{(I_{m+1}(\lambda a)J_m(\lambda a) + I_m(\lambda a)J_{m+1}(\lambda a))(K_m(\lambda\rho_2)Y_m(\lambda a) - K_m(\lambda a)Y_m(\lambda\rho_2))}{\{J'_m(\lambda a)Y_m(\lambda a) + (2/\pi)I'_m(\lambda a)K_m(\lambda a)\}}\right)$$
$$\times (a_m \cos m\phi_2 + b_m \sin m\phi_2). \tag{41}$$

Table 1
T he radius of failure points ρ_f for each spurious frequency λ_s satisfying $K_m(\lambda_s a)Y_{m+1}(\lambda_s a) - K_{m+1}(\lambda_s a)Y_m(\lambda_s a) = 0$ in the transverse displacement constraint [$K_m(\lambda_s\rho_f)Y_m(\lambda_s a) - K_m(\lambda_s a)Y_m(\lambda_s\rho_f) = 0$]

No.	Frequency (λ_s)	Mode type[a]	ρ_{f1}	ρ_{f2}	ρ_{f3}	ρ_{f4}
1	1.42796	(1,0)	3.81005	6.01947	8.22795	10.4327
2	2.63016	(2,0)	2.58583	3.81087	5.02250	6.22735
3	3.17058	(0,0)	2.23941	3.22393	4.21410	5.20439
4	3.78094	(3,0)	2.14307	3.01415	3.86758	4.71271
5	4.64695	(1,1)	1.85261	2.52824	3.20586	3.88285
6	4.90423	(4,0)	1.90970	2.59573	3.26242	3.91997

[a]In mode type (m, n), m denotes the number of diametrical nodes and n denotes the number of circular nodes for interior mode and wave numbers for exterior mode, respectively.

Table 2
T he radius of failure points ρ_f for each spurious frequency λ_s satisfying $K_m(\lambda_s a)Y_{m+1}(\lambda_s a) - K_{m+1}(\lambda_s a)Y_m(\lambda_s a) = 0$ in the normal derivative constraint [$K_m(\lambda_s a)Y_{m-1}(\lambda_s\rho_f) + K_{m-1}(\lambda_s\rho_f)Y_m(\lambda_s a) + K_{m+1}(\lambda_s\rho_f)Y_m(\lambda_s a) - K_m(\lambda_s a)Y_{m+1}(\lambda_s\rho_f) = 0$]

No.	Frequency(λ_s)	Mode type	ρ_{f1}	ρ_{f2}	ρ_{f3}	ρ_{f4}
1	1.42796	(1,0)	2.51699	4.86297	7.08935	9.30402
2	2.63016	(2,0)	1.87589	3.17561	4.40054	5.61216
3	3.17058	(0,0)	1.68407	2.71224	3.70564	4.69865
4	3.78094	(3,0)	1.63880	2.56548	3.43099	4.28213
5	4.64695	(1,1)	1.47590	2.17915	2.85900	3.53782
6	4.90423	(4,0)	1.51197	2.24418	2.92232	3.58557

Please cite this article as: Lee WM, Chen JT. Analytical study and numerical experiments of true and spurious eigensolutions of free vibration of circular plates using real-part.... Eng Anal Bound Elem (2007), doi:10.1016/j.enganabound.2007.09.004

Collecting the coefficients of a_m and b_m in Eqs. (40) and (41), we have

$$[W] = \begin{bmatrix} \cos(m\phi_1) & \sin(m\phi_1) \\ \cos(m\phi_2) & \sin(m\phi_2) \end{bmatrix}. \tag{42}$$

If the determinant of the matrix $[W]$ is zero, then Eqs. (40) and (41) do not provide two independent constraints for a_m and b_m. In this case, the intersection angle $(\phi_1 - \phi_2)$ between the two selected points satisfying

$$\sin(m(\phi_1 - \phi_2)) = 0 \quad \text{or} \quad \phi_1 - \phi_2 = \frac{n\pi}{m}, \quad m = 1, 2, 3 \ldots, \quad n = 0, 1, 2, 3 \ldots \tag{43}$$

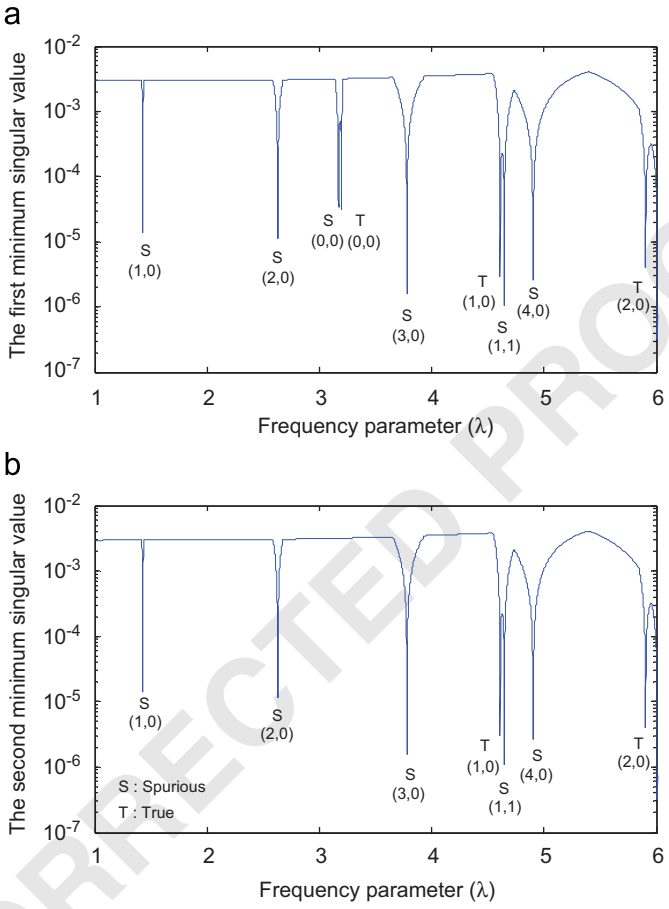

Fig. 1. The first and second minimum singular values σ_1 and σ_2 vs. λ for a circular clamped plate using the real-part U, Θ boundary integral equation

Table 3
The former nine frequency parameters (λ) for the clamped circular plate

Mode	Analytic method	Semi-analytic method	ABAQUS	Mode type
1	1.4280(S)	1.4280	N/A	(1,0)
2	2.6302(S)	2.6300	N/A	(2,0)
3	3.1706(S)	3.1710	N/A	(0,0)
4	3.1962(T)	3.1960	3.1967	(0,0)
5	3.7809(S)	3.7810	N/A	(3,0)
6	4.6109(T)	4.6110	4.6124	(1,0)
7	4.6470(S)	4.6470	N/A	(1,1)
8	4.9042(S)	4.9040	N/A	(4,0)
9	5.9057(T)	5.9060	5.9080	(2,0)

S: spurious T: true.

Please cite this article as: Lee WM, Chen JT. Analytical study and numerical experiments of true and spurious eigensolutions of free vibration of circular plates using real-part.... Eng Anal Bound Elem (2007), doi:10.1016/j.enganabound.2007.09.004

makes the two equations dependent. Besides, the radius ρ_1 and ρ_2 in CHEEF points (ρ_1, ϕ_1) and (ρ_2, ϕ_2) should not make the bracket in both Eqs. (37) and (38) be zero. Therefore, we must avoid these failure points in order to effectively filter out the spurious eigenvalues of multiplicity two.

By moving the field point x to be the CHEEF point outside the domain for the clamped case, we have

$$\begin{bmatrix} U^C\Theta^C \\ U^C_\theta\Theta^C_\theta \end{bmatrix}_{2N_C\times 4N} \begin{Bmatrix} v \\ m \end{Bmatrix}_{4N\times 1} = \begin{Bmatrix} 0 \\ \vdots \\ 0 \end{Bmatrix}_{4N\times 1}, \tag{44}$$

where the superscript C denotes the CHEEF point in the null-field equation and the subscript $N_c(\geqslant 1)$ indicates the number of additional CHEEF points. Combining Eqs. (35) and (44) together to obtain the overdetermined system, we have

$$\begin{bmatrix} U\Theta \\ U_\theta\Theta_\theta \\ U^C\Theta^C \\ U^C_\theta\Theta^C_\theta \end{bmatrix}_{(4N+2N_C)\times 4N} \begin{Bmatrix} v \\ m \end{Bmatrix}_{4N\times 1} = \begin{Bmatrix} 0 \\ \vdots \\ 0 \end{Bmatrix}_{(4N+2N_C)\times 1}. \tag{45}$$

Therefore, an overdetermined system is obtained to ensure a unique solution through SVD detection.

The concept of the CHEEF method and SVD technique of updating term are the same in constructing an overdetermined system to obtain a unique solution. From the view point of computation, CHEEF method used the minimum number of dimensions than that of the SVD technique of updating term using dual equations although it may take the risk for the failure of the CHEEF points. In other words, it works to overcome the spurious eigenproblem by using only real-part formulation under the condition that we provide sufficient constraints by adding the CHEEF points. It is

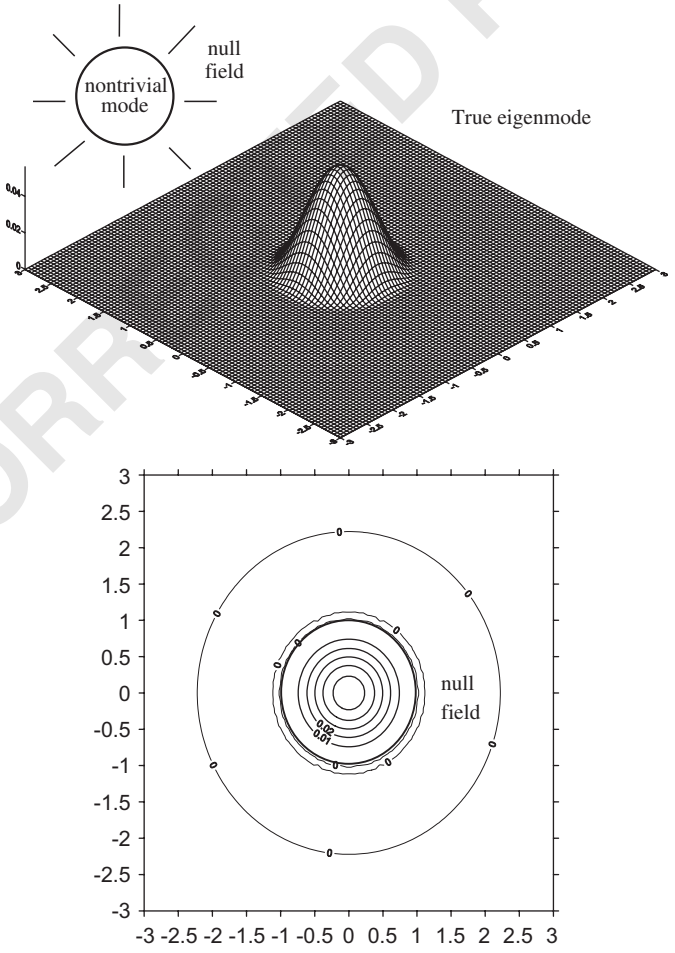

Fig. 2. The displacement 3D wire flame and 2D contour plot of the true mode (0,0) of a circular clamped plate with $\lambda_s = 3.196$.

Please cite this article as: Lee WM, Chen JT. Analytical study and numerical experiments of true and spurious eigensolutions of free vibration of circular plates using real-part.... Eng Anal Bound Elem (2007), doi:10.1016/j.enganabound.2007.09.004

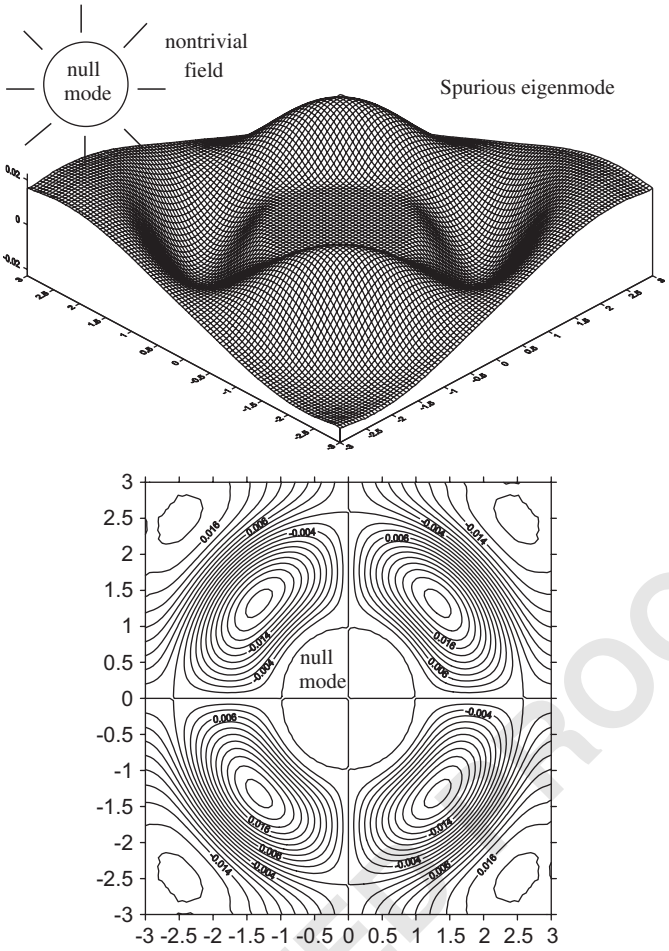

Fig. 3. The displacement 3D wire flame and 2D contour plot of the spurious mode (2,0) of a circular clamped plate with $\lambda_s = 2.630$.

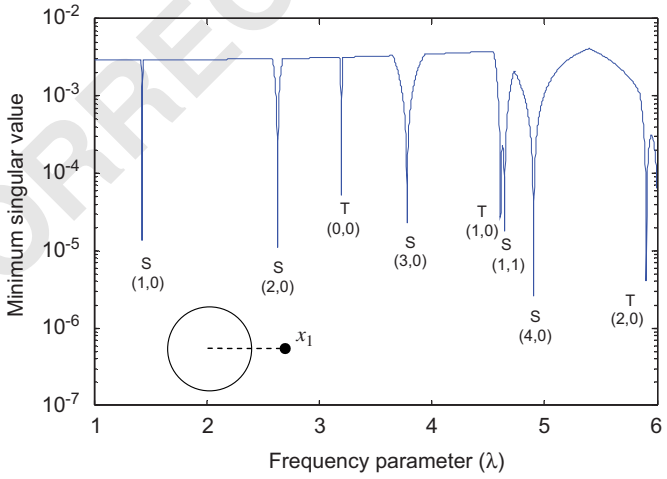

Fig. 4. The first minimum singular values σ_1 vs. λ using a CHEEF point x_1 (1.4, 0.0) with displacement constraint.

well known that kernels of real and imaginary parts are not fully independent and obey Hilbert transform. Therefore, complex-valued BEM is not the optimal approach since it overlooks the Hilbert transform pair and causes much unnecessary computation. From the viewpoint of computational cost, real-part kernel approach in conjunction with selected CHEEF points is the best one.

Please cite this article as: Lee WM, Chen JT. Analytical study and numerical experiments of true and spurious eigensolutions of free vibration of circular plates using real-part.... Eng Anal Bound Elem (2007), doi:10.1016/j.enganabound.2007.09.004

4. Numerical examples

For the numerical experiment, we considered a circular plate with the Poisson ratio $v = \frac{1}{3}$ and the radius of one meter ($a = 1$ m) subjected to the clamped boundary condition. The CHEEF method was employed to filter out the spurious eigenvalues and to check the validity of the mathematical analysis in the following examples.

4.1. True and spurious eigenvalues and modes

By taking six terms in the Fourier series for $m(s)$ and $v(s)$, the semi-analytical method is employed to solve the natural frequency parameters and natural modes. Figs. 1(a) and (b) show the first and the second minimum singular values of the influence matrix shown in Eq. (35) versus the frequency parameter λ. In the range of $0 \leqslant \lambda \leqslant 6$, we have three true

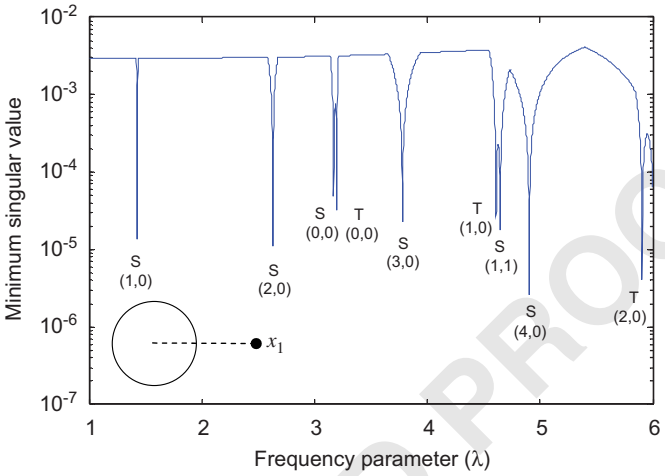

Fig. 5. The first minimum singular values σ_1 vs. λ using a CHEEF point x_1 (2.2394, 0.0) with displacement constraint.

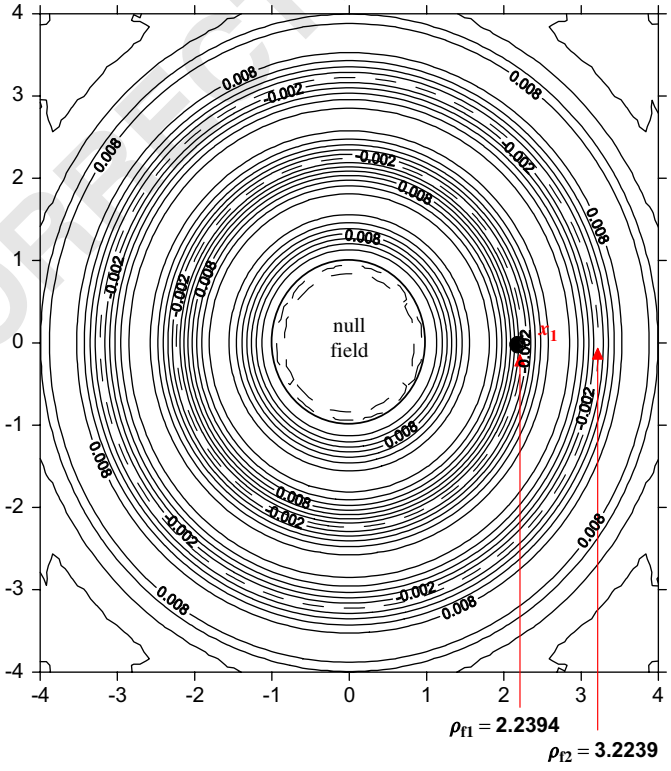

Fig. 6. The displacement contour plot of the spurious mode (0,0) of a circular clamped plate with $\lambda_s = 3.171$.

Please cite this article as: Lee WM, Chen JT. Analytical study and numerical experiments of true and spurious eigensolutions of free vibration of circular plates using real-part.... Eng Anal Bound Elem (2007), doi:10.1016/j.enganabound.2007.09.004

eigenvalues [3.1962,4.6109 and 5.9057] and six spurious eigenvalues [1.4280, 2.6302, 3.1706, 3.7809, 4.6470 and 4.9042]. All are repeated eigenvalues, except for the eigenvalue 3.1706 and 3.1962. Since the direct-searching scheme [19] is used, the drop location indicates the possible eigenvalue. The simultaneous appearance of drop indicates the multiplicities as given in Fig. 1(b). This case was also solved by using the FEM software (ABAQUS) [29] with 8668 elements and 8818 nodes. In addition to the results of semi-analytic method and finite element method using ABAQUS, Table 3 also lists the analytic results of the true and spurious frequency parameters according to the eigenequation in Eq. (34). It is observed that the spurious frequency parameters were not found in the results of the finite element method. The results of semi-analytical method match well with those of the analytic results. The true ($\lambda_t = 3.196$) and spurious ($\lambda_s = 2.630$) modes of a circular plate subject to clamped boundary conditions are shown in Figs. 2 and 3, respectively. The displacement field of the interior ($\rho < a$) and exterior ($\rho < a$) points of true eigenvalue mode are the nontrivial mode and null-field, respectively, as Eqs. (36) and (37) predicted. On the contrary, Fig. 3 shows the null field in the domain ($\rho < a$) and the nontrivial field for the exterior domain ($\rho > a$). The interesting results of biharmonic operator for plate here is similar to that of harmonic operator for membrane [11].

Based on this finding, we can filter out spurious eigenvalue by collocating the nonzero exterior field points in the null-field integral equation as additional constraints.

4.2. CHEEF points with displacement constraint

Fig. 4 shows σ_1 vs. λ by additionally considering Eq. (37) for collocating one exterior point $x_1(\rho_1 = 1.4, \phi_1 = 0)$. This treatment can filter out the single spurious eigenvalue of 3.171. But, after comparing with Fig. 1(b), the other repeated ones

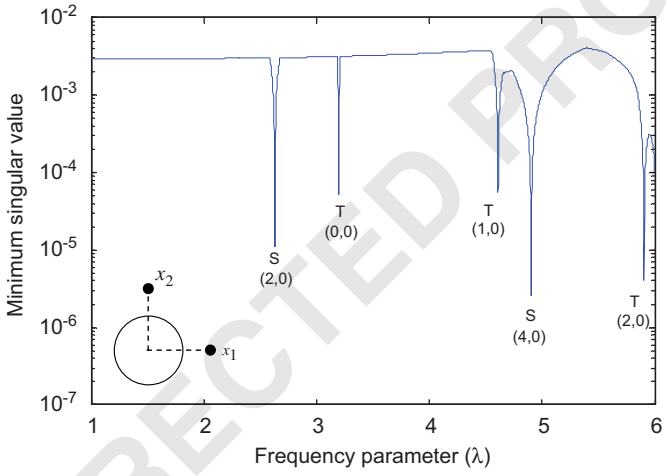

Fig. 7. The first minimum singular values σ_1 vs. λ using two CHEEF points x_1 (1.4, 0.0) and x_2 (1.4, $\pi/2$) with displacement constraint.

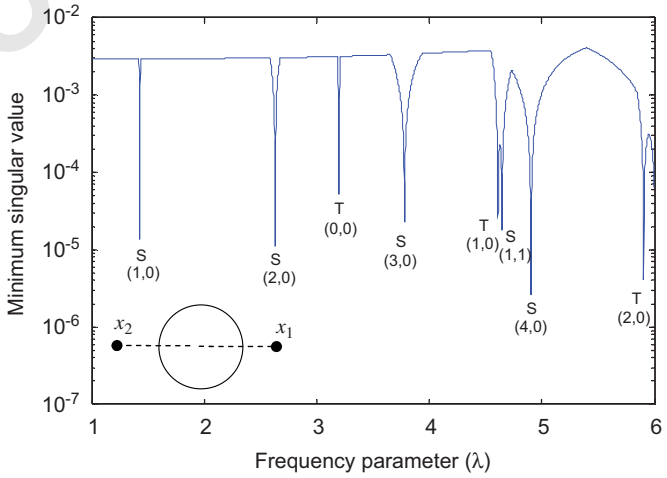

Fig. 8. The first minimum singular values σ_1 vs. λ using two CHEEF points x_1 (1.4, 0.0) and x_2 (1.4, π) with displacement constraint.

Please cite this article as: Lee WM, Chen JT. Analytical study and numerical experiments of true and spurious eigensolutions of free vibration of circular plates using real-part.... Eng Anal Bound Elem (2007), doi:10.1016/j.enganabound.2007.09.004

still appear as expected in the analytical derivation. If the collocating exterior point is located at the failure point with radius $\rho_f = 2.2394$ as shown in Table 1, which is on the circular node, then the spurious eigenvalue λ_s of 3.171 cannot be filtered out as shown in Fig. 5. The spurious eigenmode of 3.171 shown in Fig. 6 indicates two circular nodes which match well the data in Table 1, for instance, 2.2394 and 3.2239. If the additional two points $x_1(\rho_1 = 1.4, \phi_1 = 0)$ and $x_2(\rho_2 = 1.4, \phi_2 = \pi/2)$ with intersecting angle of $\pi/2$ are selected, then the mode type of the spurious eigenvalue with mode (2,0) or (4,0) cannot be filtered out as shown in Fig. 7 ($\sin(2(\pi/2) = 0, \sin(4(\pi/2) = 0$), since these modes have diametrical nodes with intersecting angle of $\pi/2$. For example, the spurious eigenvalue λ_s of 2.63 with mode (2,0) is shown in Fig. 3. Similarly, for both positions x_1 and x_2 with intersecting angle π, only the spurious eigenvalue with mode type $(0, n)$ can be filtered out as shown in Fig. 8 since no diametrical nodes in these spurious modes can be found in Fig. 6. Figs. 9 and 10 are the results by adopting three points $[x_1(\rho_1 = 1.4, \phi_1 = 0)$, $x_2(\rho_2 = 1.4, \phi_2 = \pi/2)$ and $x_3(\rho_3 = 1.4, \phi_3 = \pi)]$ and four points $[x_1(\rho_1 = 1.4, \phi_1 = 0)$, $x_2(\rho_2 = 1.4, \phi_2 = \pi/2)$, $x_3(\rho_3 = 1.4, \phi_3 = \pi)$ and $x_3(\rho_4 = 1.4, \phi_4 = 3\pi/2)]$ with different intersecting angles, respectively. It is obvious that the results of Figs. 9 and 10 are the same as that of Fig. 7. This indicates that the additional exterior points with intersecting angle satisfying Eq. (43) will not provide extra independent constraint equations and fail to filter out spurious eigenvalues. At the same time, if the additional exterior points, one point x_1 $(\rho_1 = 1.9097$, $\phi_1 = 0)$ and another point $x_2(\rho_2 = 1.4, \phi_2 = \pi/9)$, are both chosen, then the spurious roots can be filtered out, except $\lambda = 4.904$ as illustrated in Fig. 11. It is the failure point with radius $\rho_f = 1.9097$ as shown in Table 1 that cannot filter out this spurious root. The spurious eigenmode of $\lambda = 4.904$ shown in Fig. 12 indicates two circular nodes which match the data in Table 1, for instance, 1.9097 and 2.5957. Fig. 13 indicates that if the additional two exterior points $x_1(\rho_1 = 1.4, \phi_1 = 0)$ and $x_2(\rho_2 = 1.4, \phi_2 = \pi/9)$ are carefully chosen, then all the spurious eigenvalues can be filtered out.

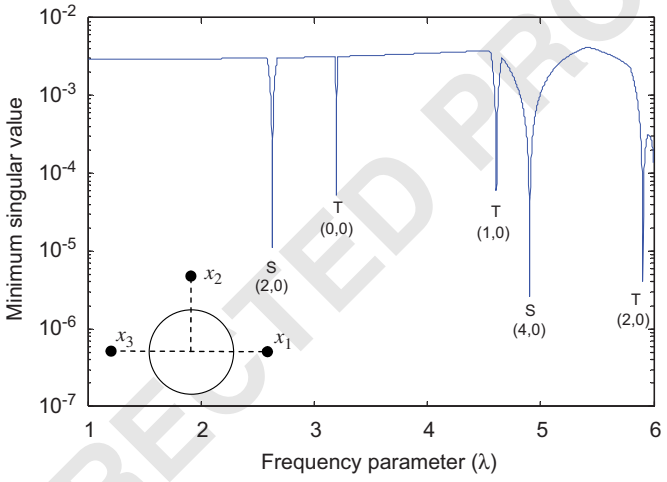

Fig. 9. The first minimum singular values σ_1 vs. λ using three CHEEF points x_1 (1.4, 0.0), x_2 (1.4, $\pi/2$) and x_3 (1.4, π) with displacement constraint.

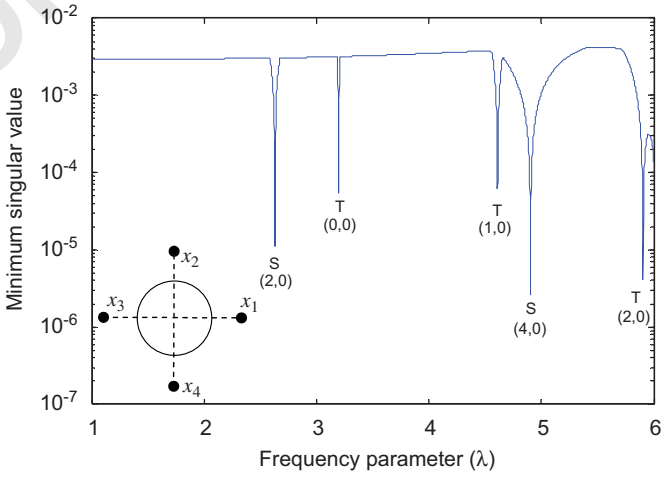

Fig. 10. The first minimum singular values σ_1 vs. λ using four CHEEF points x_1 (1.4, 0.0), x_2 (1.4, $\pi/2$), x_3 (1.4, π) and x_4 (1.4, $3\pi/2$) with displacement constraint.

Please cite this article as: Lee WM, Chen JT. Analytical study and numerical experiments of true and spurious eigensolutions of free vibration of circular plates using real-part.... Eng Anal Bound Elem (2007), doi:10.1016/j.enganabound.2007.09.004

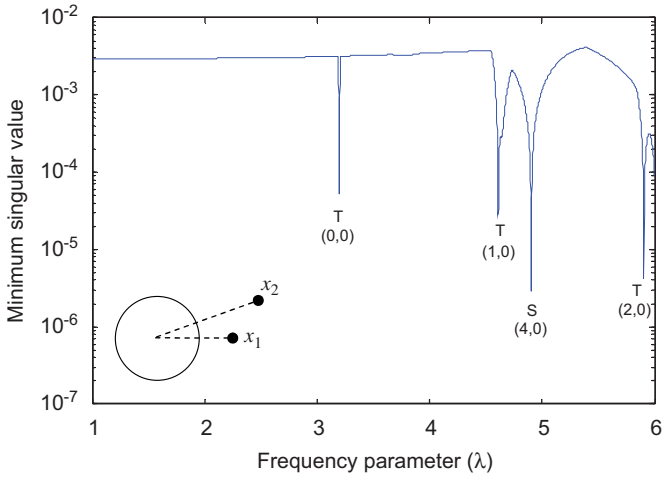

Fig. 11. The first minimum singular values σ_1 vs. λ using two CHEEF points x_1 (1.4, 0.0) and x_2 (1.9097, π/9) with displacement constraint.

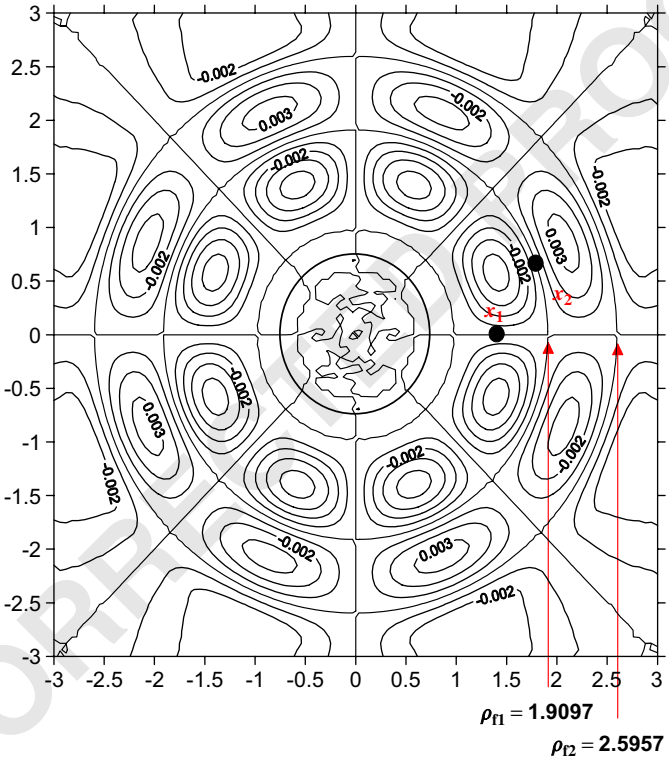

Fig. 12. The displacement contour plot of the spurious mode (4,0) of a circular clamped plate with $\lambda_s = 4.904$.

4.3. CHEEF points with normal derivative constraint

In addition to transverse displacement constraint by Eq. (37), the normal derivative constraint in Eq. (38) can be considered here. If the two exterior points, one point x_1 ($\rho_1 = 1.8759$, $\phi_1 = 0$) and another point $x_2(\rho_2 = 1.2, \phi_2 = \pi/9)$, are both chosen, then the spurious eigenvalues can be filtered out, except 2.630 as illustrated in Fig. 14. It is the failure point with radius $\rho_f = 1.8759$ as shown in Table 2 that cannot filter out this spurious root. The normal derivative contour plot of the spurious eigenmode of 2.630 as shown in Fig. 15 indicates two circular nodes which match well the data in Table 2, for instance, 1.8759 and 3.1756. As the results of the displacement constraint shown in Fig. 13, all the spurious

Please cite this article as: Lee WM, Chen JT. Analytical study and numerical experiments of true and spurious eigensolutions of free vibration of circular plates using real-part.... Eng Anal Bound Elem (2007), doi:10.1016/j.enganabound.2007.09.004

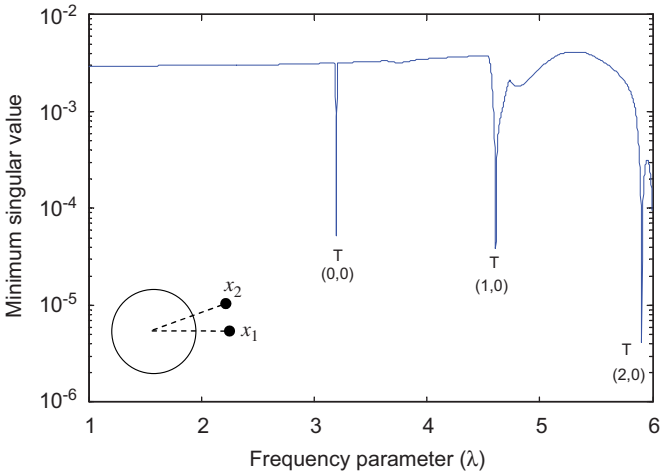

Fig. 13. The first minimum singular values σ_1 vs. λ using two CHEEF points x_1 (1.4, 0.0) and x_2 (1.4, $\pi/9$) with displacement constraint.

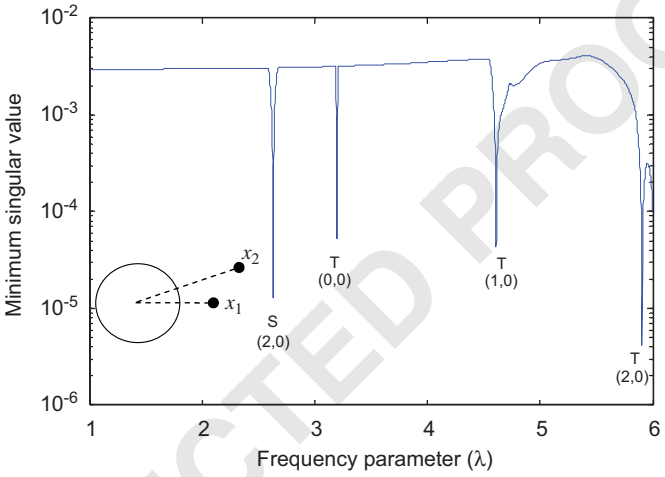

Fig. 14. The first minimum singular values σ_1 vs. λ using two CHEEF points x_1 (1.2, 0) and x_2 (1.8759, $\pi/9$) with normal derivative constraint.

eigenvalues can be filtered out by employing the normal derivative constraints, as presented in Fig. 16, if the two exterior points $x_1(\rho_1 = 1.2, \phi_1 = 0)$ and $x_2(\rho_2 = 1.2, \phi_2 = \pi/9)$ are carefully chosen.

4.4. CHEEF points with tangent derivative constraint

Instead of employing normal derivative constraints, the tangent derivative constraint in Eq. (39) is considered. The situation is quite different. As expected in the trivial ($m = 0$) tangent derivative constraint of Eq. (39), Fig. 17 indicates that wherever the position of collocating points were chosen or two more CHEEF points were added, the spurious eigenvalue with mode (0, n), such as $\lambda_s = 3.171$ with (0, 0), cannot be filtered. The tangent derivative contour plot of the spurious eigenmode of $\lambda_s = 3.171$ shown in Fig. 18 indicates a null field in the full plane, so the tangent derivative constraint cannot provide the independent constraint for the spurious eigenvalues with mode (0, n) due to the axial symmetric configuration.

4.5. CHEEF points with mixed-type constraints

As stated previously, the repeated spurious eigenvalues can be filtered out by collocating two independent exterior points which must avoid satisfying Eq. (43). Free of checking the intersection angle, we can consider the mixed-type constraints, such as combining displacement and normal derivative constraint at the same time. Fig. 19 shows σ_1 vs. λ by additionally considering displacement constraint of Eq. (37) and normal derivative constraint of Eq. (38) for one exterior collocating point $x_1(\rho_1 = 1.4, \phi_1 = 0)$. Although two constraints are involved, all spurious eigenvalues except 3.171 still appear by this combined constraint. Since this collocating point is on the diametrical node, the normal derivative at this point is definitely

Please cite this article as: Lee WM, Chen JT. Analytical study and numerical experiments of true and spurious eigensolutions of free vibration of circular plates using real-part.... Eng Anal Bound Elem (2007), doi:10.1016/j.enganabound.2007.09.004

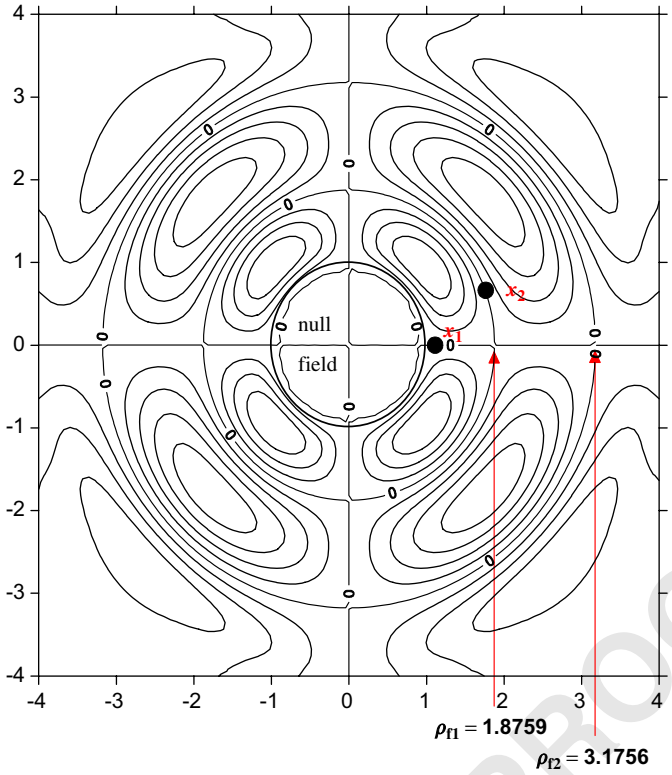

Fig. 15. The normal derivative contour plot of the spurious mode (2,0) of a circular clamped plate with $\lambda_s = 2.630$.

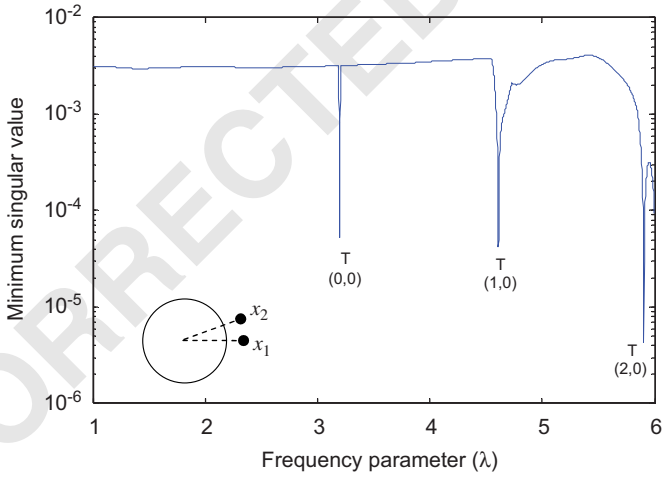

Fig. 16. The first minimum singular values σ_1 vs. λ using two CHEEF points x_1 (1.2, 0) and x_2 (1.2, π/9) with normal derivative constraint.

zero. Therefore this normal derivative constraint cannot offer independent constraint. Fig. 20 shows σ_1 vs. λ by additionally considering Eqs. (38) and (39) for collocating one exterior point $x_1(\rho_1 = 1.4, \phi_1 = 0)$. Fig. 21 shows σ_1 vs. λ by additionally considering Eqs. (37) and (39) for collocating one exterior point $x_1(\rho_1 = 1.4, \phi_1 = 0)$. From the results of figures above, we only keep the collocating point far away from the failure points as listed in Tables 1 and 2 and then all the spurious eigenvalues can be easily and efficiently filtered out.

5. Conclusions

Spurious eigensolutions of plate vibration stemming from the real-part BIEM were examined. By adopting the CHEEF method, constraints from the null-field equation are employed to deal with the problem of spurious solutions. The

Please cite this article as: Lee WM, Chen JT. Analytical study and numerical experiments of true and spurious eigensolutions of free vibration of circular plates using real-part.... Eng Anal Bound Elem (2007), doi:10.1016/j.enganabound.2007.09.004

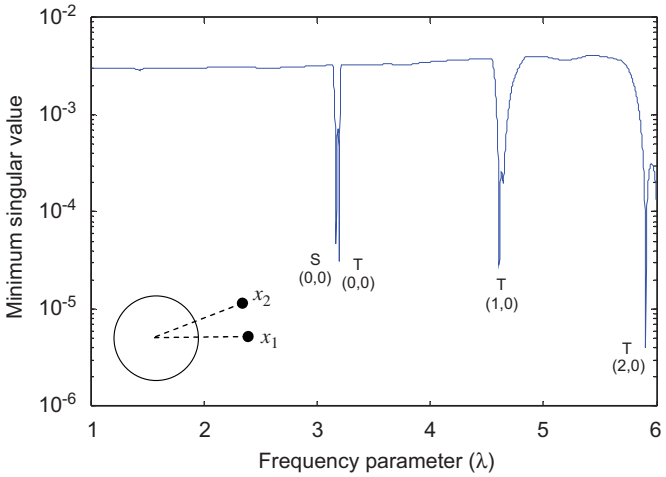

Fig. 17. The first minimum singular values σ_1 vs. λ using two CHEEF points x_1 (1.6, 0) and x_2 (1.6, π/9) with tangent derivative constraint.

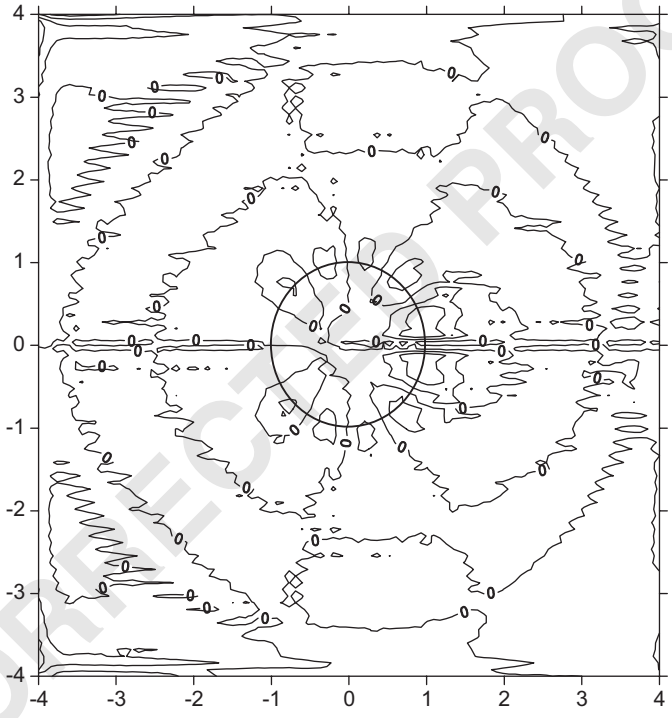

Fig. 18. The tangent derivative contour plot of the spurious mode (0,0) of a circular clamped plate with $\lambda_s = 3.171$.

constraint equations in transverse displacement and its normal and tangent derivatives for the CHEEF points in the circular plate were derived. The failure CHEEF points in selecting the exterior collocating points for circular plate were derived analytically and demonstrated numerically. If the constraints of transverse displacement, normal derivative and tangent derivative are properly chosen, one collocating point was enough to filter out all the spurious eigenvalues easily and efficiently, even for the repeated spurious eigenvalues. The CHEEF method can obviously reduce memory storage and computation time in comparison with those using other approaches. Although the circular case lacks generality, it leads to significant insight into the occurring mechanism of spurious eigensolution. It is also a great help to researchers who may require an analytical explanation as to why spurious eigensolutions occur and how they can be suppressed.

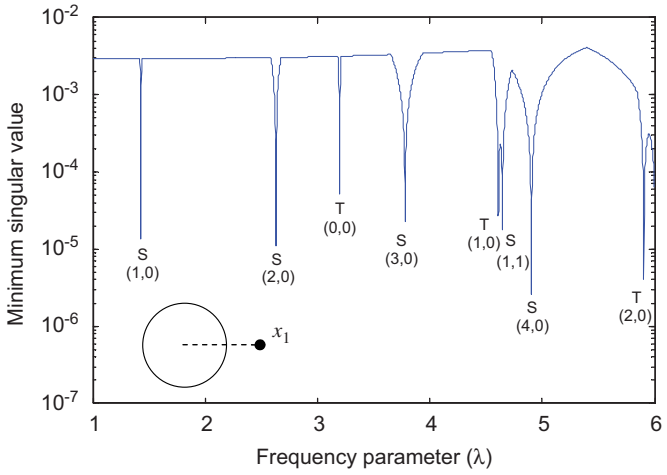

Fig. 19. The first minimum singular values σ_1 vs. λ using one CHEEF point x_1 (1.4, 0) with both displacement and normal derivative constraints.

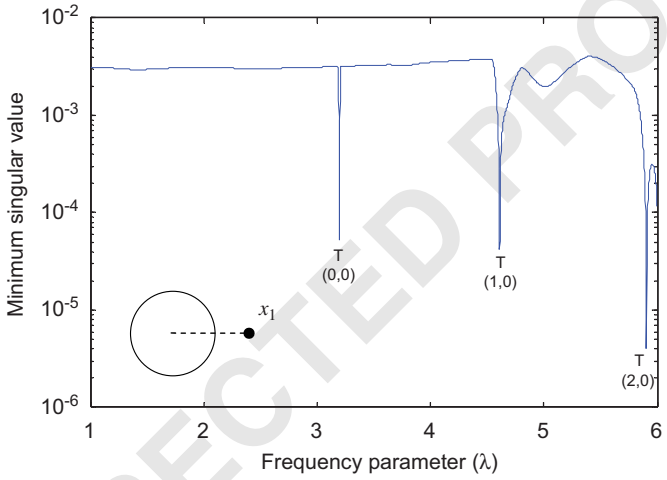

Fig. 20. The first minimum singular values σ_1 vs. λ using one CHEEF point x_1 (1.4, 0) with both normal and tangent derivative constraints.

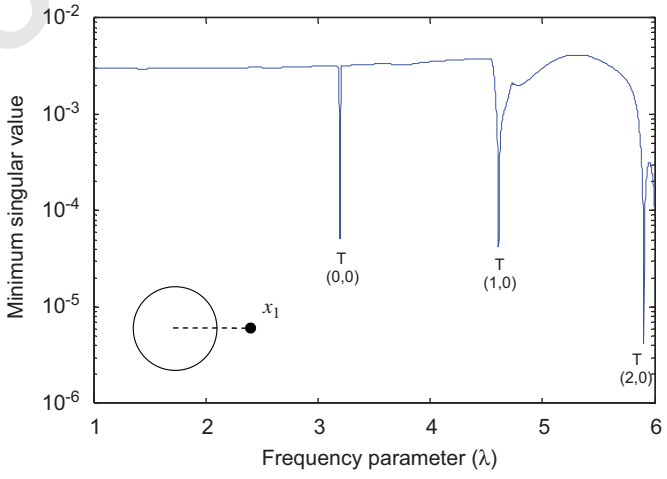

Fig. 21. The first minimum singular values σ_1 vs. λ using one CHEEF point x_1 (1.4, 0) with both displacement and tangent derivative constraints.

Please cite this article as: Lee WM, Chen JT. Analytical study and numerical experiments of true and spurious eigensolutions of free vibration of circular plates using real-part.... Eng Anal Bound Elem (2007), doi:10.1016/j.enganabound.2007.09.004

Appendix A. Degenerate kernels

$$M^1(s,x)=\frac{1}{8\lambda^2}\sum_{m=0}^{\infty}\varepsilon_m\left\{J_m(\lambda\rho)\alpha_m^Y(\lambda R)+\frac{2}{\pi}I_m(\lambda\rho)\alpha_m^K(\lambda R)\right\}\cos(m(\theta-\phi))=\sum_{m=0}^{\infty}p_{1m}\cos(m(\theta-\phi)),$$

$$M^2(s,x)=\frac{1}{8\lambda^2}\sum_{m=0}^{\infty}\varepsilon_m\left\{\alpha_m^J(\lambda R)Y_m(\lambda\rho)+\frac{2}{\pi}\alpha_m^I(\lambda R)K_m(\lambda\rho)\right\}\cos(m(\theta-\phi))=\sum_{m=0}^{\infty}p_{2m}\cos(m(\theta-\phi)),$$

where

$$p_{1m}=\frac{1}{8\lambda^2}\varepsilon_m\left\{J_m(\lambda\rho)\alpha_m^Y(\lambda R)+\frac{2}{\pi}I_m(\lambda\rho)\alpha_m^K(\lambda R)\right\},$$

$$p_{2m}=\frac{1}{8\lambda^2}\varepsilon_m\left\{\alpha_m^J(\lambda R)Y_m(\lambda\rho)+\frac{2}{\pi}\alpha_m^I(\lambda R)K_m(\lambda\rho)\right\},$$

$$\alpha_m^Y(\lambda R)=\lambda^2Y_m''(\lambda R)+\nu\left[\frac{\lambda}{R}Y_m'(\lambda R)-\frac{m^2}{R^2}Y_m(\lambda R)\right],$$

$$\alpha_m^J(\lambda R)=\lambda^2J_m''(\lambda R)+\nu\left[\frac{\lambda}{R}J_m'(\lambda R)-\frac{m^2}{R^2}J_m(\lambda R)\right],$$

$$\alpha_m^K(\lambda R)=\lambda^2K_m''(\lambda R)+\nu\left[\frac{\lambda}{R}K_m'(\lambda R)-\frac{m^2}{R^2}K_m(\lambda R)\right],$$

$$\alpha_m^I(\lambda R)=\lambda^2I_m''(\lambda R)+\nu\left[\frac{\lambda}{R}I_m'(\lambda R)-\frac{m^2}{R^2}I_m(\lambda R)\right],$$

$$\varepsilon_m=\begin{cases}1 & m=0,\\ 2 & m\neq0,\end{cases}$$

where the superscripts 1 and 2 denote the interior domain (i.e. $\rho<R$) and the exterior domain (i.e.$\rho>R$), respectively.

$$V^1(s,x)=\frac{1}{8\lambda^2}\sum_{m=0}^{\infty}\varepsilon_m\left\{J_m(\lambda\rho)\beta_m^Y(\lambda R)+\frac{2}{\pi}I_m(\lambda\rho)\beta_m^K(\lambda R)\right\}\cos(m(\theta-\phi))=\sum_{m=0}^{\infty}q_{1m}\cos(m(\theta-\phi)),$$

$$V^2(s,x)=\frac{1}{8\lambda^2}\sum_{m=0}^{\infty}\varepsilon_m\left\{\beta_m^J(\lambda R)Y_m(\lambda\rho)+\frac{2}{\pi}\beta_m^I(\lambda R)K_m(\lambda\rho)\right\}\cos(m(\theta-\phi))=\sum_{m=0}^{\infty}q_{2m}\cos(m(\theta-\phi)),$$

where

$$q_{1m}=\frac{1}{8\lambda^2}\varepsilon_m\left\{J_m(\lambda\rho)\beta_m^Y(\lambda R)+\frac{2}{\pi}I_m(\lambda\rho)\beta_m^K(\lambda R)\right\},$$

$$q_{2m}=\frac{1}{8\lambda^2}\varepsilon_m\left\{\beta_m^J(\lambda R)Y_m(\lambda\rho)+\frac{2}{\pi}\beta_m^I(\lambda R)K_m(\lambda\rho)\right\},$$

$$\beta_m^Y(\lambda R)=\lambda^3Y_m'''(\lambda R)+\frac{\lambda^2}{R}Y_m''(\lambda R)-\frac{\lambda}{R^2}[1+(2-\nu)m^2]Y_m'(\lambda R)+\left[\frac{(3-\nu)m^2}{R^3}\right]Y_m(\lambda R),$$

$$\beta_m^J(\lambda R)=\lambda^3J_m'''(\lambda R)+\frac{\lambda^2}{R}J_m''(\lambda R)-\frac{\lambda}{R^2}[1+(2-\nu)m^2]J_m'(\lambda R)+\left[\frac{(3-\nu)m^2}{R^3}\right]J_m(\lambda R),$$

$$\beta_m^K(\lambda R)=\lambda^3K_m'''(\lambda R)+\frac{\lambda^2}{R}K_m''(\lambda R)-\frac{\lambda}{R^2}\left[1+(2-\nu)m^2\right]K_m'(\lambda R)+\left[\frac{(3-\nu)m^2}{R^3}\right]K_m(\lambda R),$$

$$\beta_m^I(\lambda R)=\lambda^3I_m'''(\lambda R)+\frac{\lambda^2}{R}I_m''(\lambda R)-\frac{\lambda}{R^2}[1+(2-\nu)m^2]I_m'(\lambda R)+\left[\frac{(3-\nu)m^2}{R^3}\right]I_m(\lambda R),$$

$$\varepsilon_m=\begin{cases}1, & m=0,\\ 2, & m\neq0,\end{cases}$$

where the superscripts 1 and 2 denote the interior domain (i.e. $\rho<R$) and the exterior domain (i.e. $\rho>R$), respectively.

Please cite this article as: Lee WM, Chen JT. Analytical study and numerical experiments of true and spurious eigensolutions of free vibration of circular plates using real-part.... Eng Anal Bound Elem (2007), doi:10.1016/j.enganabound.2007.09.004

References

[1] Chen JT, Chen IL, Chen KH. Treatment of rank deficiency in acoustics using SVD. J Comput Acoust 2006;14(2):157–83.
[2] De Mey G. Calculation of the Helmholtz equation by an integral equation. Int J Numer Methods Eng 1976;10:59–66.
[3] De Mey G. A simplified integral equation method for the calculation of the eigenvalues of Helmholtz equation. Int J Numer Methods Eng 1977;11:1340–2.
[4] Yas'ko M. BEM with the real-valued fundamental solutions for the Helmholtz equation. in: Proceedings of seventh international congress on sound and vibration, Germany 2000:2037–44.
[5] Hutchinson JR. Determination of membrane vibrational characteristics by the boundary-integral equation method. In: Brebbia CA, editor. Recent advances in boundary element methods. London: Pentech Press; 1978. p. 301–15.
[6] Hutchinson JR, Wong GKK. The boundary element method for plate vibrations. In: Proceedings of the ASCE seventh conference on electronic computation. St. Louis, Missouri, New York: ASCE; 1979. p. 297–311.
[7] Hutchinson JR. An alternative BEM formulation applied to membrane vibrations. In: Brebbia CA, Maier G, editors. Boundary elements VII. Berlin: Springer; 1985.
[8] Hutchinson JR. Analysis of plates and shells by boundary collocation. In: Beskos DE, editor. Boundary elements analysis of plates and shells. Berlin: Springer; 1991. p. 314–68.
[9] Shaw RP. Boundary integral equation methods applied to wave problems. In: Banerjee PK, Shaw RP, editors. Developments in boundary element methods-1. Barking: Applied Science Publishers; 1979.
[10] Hutchinson JR. Vibration of plates. In: Brebbia CA, editor. Boundary elements X. Berlin: Springer; 1988. p. 415–30.
[11] Kuo SR, Chen JT, Huang CX. Analytical study and numerical experiments for true and spurious eigensolutions of a circular cavity using the real-part dual BEM. Int J Numer Methods Eng 2000;48:1401–22.
[12] Niwa Y, Kobayash S, Kitahara M. Determination of eigenvalues by boundary element methods. In: Banerjee PK, Shaw RP, editors. Developments in boundary element method-2. New York, NY: Applied Science Publishers; 1982. p. 143–76.
[13] Chen JT. Recent development of dual BEM in acoustic problems. Comput Methods Appl Mech Eng 2000;188(3–4):833–45.
[14] Chang JR, Yeih W, Chen JT. Determination of natural frequencies and natural modes using the dual BEM in conjunction with the domain partition technique. Comput Mech 1999;24(1):29–40.
[15] Chen JT, Huang CX, Chen KH. Determination of spurious eigenvalues and multiplicities of true eigenvalues using the real-part dual BEM. Comput Mech 1999;24(1):41–51.
[16] Chen IL, Chen JT, Kuo SR, Liang MT. A new method for true and spurious eigensolutions of arbitrary cavities using the combined Helmholtz exterior integral equation formulation method. J Acoust Soc Am 2001;109(3):982–98.
[17] Chen JT, Lin JH, Kuo SR, Chyuan SW. Boundary element analysis for the Helmholtz eigenvalue problems with a multiply connected domain. Proc R Soc London, Ser A 2001;457:2521–46.
[18] Chen JT, Liu LW, Hong H-K. Spurious and true eigensolutions of Helmholtz BIEs and BEMs for a multiply-connected problem. Proc R Soc London, Series A 2003;459:1891–924.
[19] Kitahara M. Boundary integral equation methods in eigenvalue problems of elastodynamics and thin plates. Amsterdam: Elsevier; 1985.
[20] Beskos DE. Boundary element methods in dynamic analysis. Appl Mech Rev 1987;40:1–23.
[21] Beskos DE. Boundary element methods in dynamic analysis: part II (1986–1996). Appl Mech Rev 1997;50(3):149–97.
[22] Chen JT, Wong FC. Analytical derivations for one-dimensional eigenproblems using dual BEM, MRM. Eng Anal Boundary Element 1997;20(1):25–33.
[23] Chen JT, Huang CX, Wong FC. Determination of spurious eigenvalues and multiplicities of true eigenvalues in the dual multiple reciprocity method using the singular value decomposition technique. J Sound Vibration 2000;230(2):203–19.
[24] Schenck HA. Improved integral formulation for acoustic radiation problems. J Acoust Soc Am 1968;44(1):41–58.
[25] Chen JT, Lin SY, Chen IL, Lee YT. Mathematical analysis and numerical study to free vibrations of annular plates using BIEM and BEM. Int J Numer Methods Eng 2006;65:236–63.
[26] Chen JT, Hsiao CC, Leu SY. Null-field integral equation approach for plate problems with circular boundaries. JAppl Mech 2006;73:679–93.
[27] IMSL Math/Library Volumes 1 and 2 version 4.01 Visual Numerics, Inc., 1999.
[28] Leissa AW. Vibration of plates. NASA SP-160, 1969.
[29] ABAQUS/CAE 6.5 Hibbitt, Karlsson and Sorensen, Inc., RI, 2004.

Please cite this article as: Lee WM, Chen JT. Analytical study and numerical experiments of true and spurious eigensolutions of free vibration of circular plates using real-part.... Eng Anal Bound Elem (2007), doi:10.1016/j.enganabound.2007.09.004